IEEE Access
Multidisciplinary | Rapid Review | Open Access Journal

Received 8 May 2023, accepted 26 May 2023, date of publication 30 May 2023, date of current version 14 June 2023.

Digital Object Identifier 10.1109/ACCESS.2023.3281453

RESEARCH ARTICLE

Detection of Depression Using Weighted Spectral Graph Clustering With EEG Biomarkers

SHREEYA GARG[1], URVASHI PRAKASH SHUKLA[2], AND LINGA REDDY CENKERAMADDI[3], (Senior Member, IEEE)

[1]Department of Electronics, Banasthali Vidyapith, Radha Kishanpura 304022, India
[2]Department of Computer Science, Banasthali Vidyapith, Radha Kishanpura 304022, India
[3]Department of Information and Communication Technology, University of Agder, 4879 Grimstad, Norway

Corresponding author: Linga Reddy Cenkeramaddi (linga.cenkeramaddi@uia.no)

This work was supported by the International Partnerships for Excellent Education, Research and Innovation (INTPART) Program from the Research Council of Norway through the Indo–Norwegian Collaboration in Autonomous Cyber-Physical Systems (INCAPS) Project from the Research Council of Norway under Grant 287918.

ABSTRACT The alarming annual growth in the number of people affected by Major Depressive Disorder (MDD) is a problem on a global scale. In the primary scrutiny of depression, Electroencephalography (EEG) is one of the analytical tools available. Machine Learning (ML) and Deep Neural Networks (DNN) methods are the most common techniques for MDD diagnosis using EEG. However, these ML methods heavily rely on manually annotated EEG signals, which can only be generated by experts, for training. This also necessitates a large amount of memory and time constraints. The requirement of huge amounts of data to foresee emerging tendencies or undiscovered alignments is enforced. This article develops an unsupervised learning method for identifying MDD in light of these difficulties. The preprocessed EEG is used to extract three quantitative biomarkers (Band Power: Beta, Delta, and Theta), and three signal features (Detrended Fluctuation Analysis (DFA), Higuchi's Fractal Dimension (HFD), and Lempel-Ziv Complexity (LZC)). Through the extracted features, an undirected graph is created using the features as a weight along the edges, with nodes as channels in EEG recording. The bifurcation of the subjects in either of the classes (MDD or N) is done by implementing spectral clustering. A 98% accuracy with a 2.5% of miss-classification error is achieved for the left hemisphere. In contrast, a 97% accuracy with a 3.3% *CEP* (or miss-classification error or Classification Error Percentage) is achieved for the right hemisphere. FP1 and F8 channels have achieved the highest possible level of classification accuracy.

INDEX TERMS Unsupervised classification, biomarkers, bandpower, EEG signal, depression.

I. INTRODUCTION

Anxiety, irritability, and a general lack of interest in or interaction with the outside world are hallmarks of Major Depressive Disorder (MDD), a spectrum of complex and varied symptoms. In terms of prevalence and economic impact, depression is the most common mental condition worldwide, according to the World Health Organization [1]. About one in fifteen adults experience symptoms each year. Close to 264 million people all over the world are battling this silent killer. Many people all over the world were severely affected by the COVID-19 pandemic. More than half of the Indian population experiences anxiety and depression, according to a survey conducted after COVID-19 [2].

The various scales or scores are typically used to determine the diagnostic procedures for MDD. The physical therapist performing the assessments will significantly impact these measures. Investigating techniques that considerably lessen the load and automatically assist in the early detection of MDD is extremely important for researchers.

Electroencephalography (EEG) is generally used to study brain activation, particularly in physiological settings [16]. According to [17], the brain activity that the EEG measures

The associate editor coordinating the review of this manuscript and approving it for publication was Santosh Kumar.

TABLE 1. Research articles based on EEG quantitative biomarkers.

Article	Year	EEG Dataset			Biomarkers	Method	Accuracy(%)	Observations
		Total	Normal	MDD				
Livia Livint, Pop,et al. [3]	2022	57	18	39	(Delta + Theta)/(Alpha + Beta) Ratio (DTABR), respectively the Delta/Alpha Ratio (DAR)	Study of biomarkers with HADS-D subscale	-	A study conducted
Danish M. Khan,et al. [4]	2022	60	30	30	wavelet coherence	3D and 2D CCN	97.5	Traning time =9.42 mins
Molly McVoy,et al. [5]	2022	49	14	35	qEEG in four frequency bands (alpha, beta, theta, and delta)	logistic regression model	97.5	Tested on adolescents
Seal A, et al. [6]	2021	33	18	15	Resting: EEG, Notch =50 Hz	CNN-DeprNet(18 layers),HPF= 0.1-100 Hz,	91.40	Training= 37.6 mins and Testing = 0.036 sec
Chien Te Wu, et al. [7]	2021	400	200	200	HFD, Katz's Fractal Dimension (KFD),Coherence,Bandpower	KNN, Linear discriminant analysis (LDA), SVM, CK-SVM	84.16	CK-SVM Model tested with 51 features 84.16%and 62 feature set for 80.83%.
Ay B, et al. [8]	2019	30	15	15	EEG Signal	CNN-LTSM	99.12	Training Time (1 Epoch)= 52 sec
Cai H, et al. [9]	2018	213	92	121	C0-complexity, Shannon and Power Spectral Entropy, Kolmogoro,	KNN, SVM, CT and ANN	79.27	Highest accuracy: bandpower (KNN)
Bachmann M, et al. [10]	2018	26	13	13	SASI, Aplha Power Variability, Relative Gamma BP, HFD, DFA, LZC.	Logistic Regression	88.00	Subjects analyzed small, hinder the accuracy.
Mumtaz W, et al. [11]	2017	64	30	34	Wavelet Transformation(WT) Coherence	Logistic Regression (LR)	87.50	Iterations=100
Mumtaz W, et al. [12]	2016	63	30	33	Spectral bandpower and frontal alpha asymmetry	Naive Bayesian(NB), LR and SVM	98.40	Iterations=100
Acharya, et al. [13]	2015	30	15	15	Largest Lyapunov Exponent (LLE),DFA, Entropy, Hurst's Exponent.	Classifiers - SVM, KNN, NB, PNN and Decision Tree(DT)	98.00	Training = 199.07 sec (LH) and 198.68 sec (RH) for 1 Epoch each
Hosseinifard B, et al. [14]	2013	90	45	45	BP, DFA, HFD, Correlation, LLE.	Classifiers : LDA, LR, KNN.	90.00	LR Highest Accuracy.
Ahmadlou M, et al. [15]	2012	24	12	12	KFD, HFD , Wavelet analysis	Enhanced probabilistic neural network (EPNN)	91.30	Slow with large memory space

primarily reflects the neurological system and mental states. These recordings are an essential tool for understanding how the brain functions and, consequently, for diagnosing and tracking significantly impact [18] including epilepsy, insomnia, seizures, etc. EEG signals are visually complex, non-stationary, and have inherent non-linearity thus, extraction of its peculiar characteristics is a difficult task. This necessitates the use of advanced dynamic algorithms. Other difficulties include the signal's short magnitude range, which makes it susceptible to disturbances (e.g., physiological or non-physiological artifacts).

As a result, several EEG-based biomarkers can efficiently address the aforementioned problems by differentiating between healthy and MDD participants under varied therapy responses [19]. Machine Learning (ML) techniques are used for the majority of analyses that are based on classification. To verify the effectiveness of ML techniques, a sizable dataset is required. The majority of analyses for the classification are done utilizing machines. In order to evaluate the performance of the proposed algorithm using the limited EEG data available, cross-validation techniques are used, which can result in overfitting and data leaking [7]. A huge amount of labeled training data is essential for the deep learning approaches' accuracy [20]. The process of labeling EEG signals is extremely time-consuming and requires the pathologist's competence [21]. Analysis of unlabeled data, however, can be beneficial.

In this study, the authors present a method for primary EEG signal decoding of depression utilizing an unsupervised approach. Quantitative EEG biomarkers are used in the analysis in order to successfully address the difficulties and problems associated with working with raw EEG information. The framework designed is an entire system that starts with pre-processing the data and extracts six carefully selected EEG-based features to accurately describe the signal. To decode the patients into two categories—Normal and MDD—these features are converted into a weighted graph and spectral clustering minutely segregates the nodes through weights associated. The full layout of the created framework is displayed in Fig.1.

The following are the major contributions:

- The developed framework is a fully unsupervised method to predict MDD, doing away without labeling and reliance on the expert directly. Additionally, the complexity of calculation and time (in terms of train and test time of a model designed) are both considerably lowered. To effectively handle problems like overfitting and data leaking, the dependency on the large data set is effectively decreased.

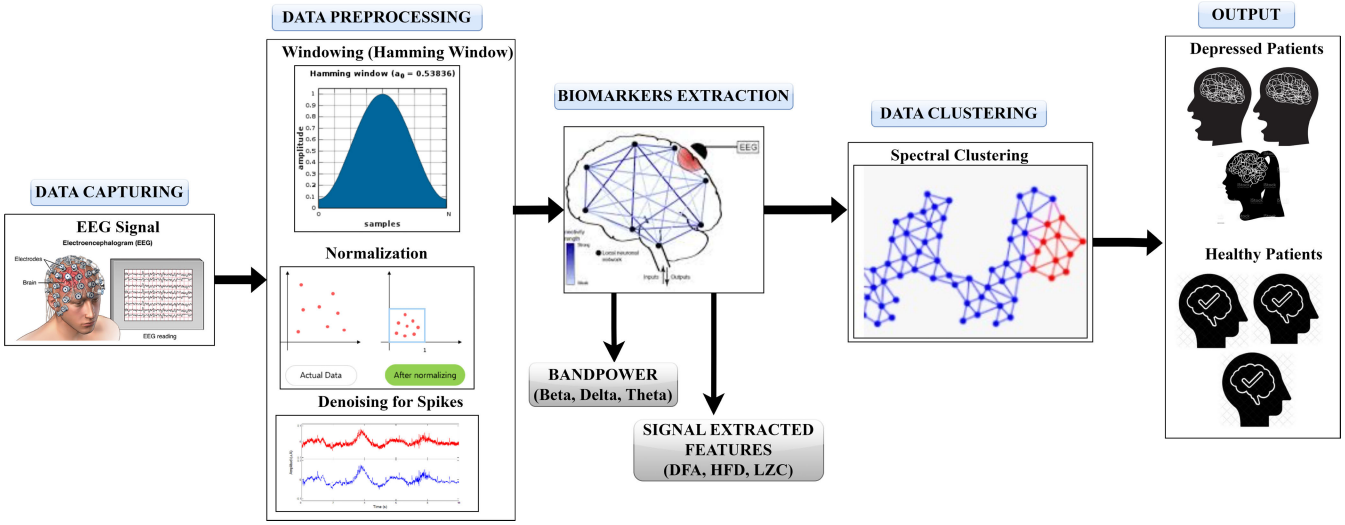

FIGURE 1. Comprehensive proposed framework for MDD.

- Through electrodes, the neural data collected at various frequencies from various brain regions can be translated into cortical activity. The developed system is dependent on the signal extraction characteristics and the resulting quantitative EEG biomarkers. It is commendable that the challenge of working with a direct EEG signal is addressed. Additionally, by employing signal-derived features, non-stationary and non-linear EEG properties can be effectively examined.
- To comprehend the relationship and interdependency between the inter and intra-hemispheric electrode pairs, a thorough analysis is conducted. Also, the author has used spatial and temporal reliance as a function of the particular channel.
- The computational complexity and time required by the suggested framework are lower than those of the current deep neural network methods. Where C is the total number of channels, the computational complexity of the spectral clustering is $O(C^3)$.

The paper is structured as follows: In Section II, a complete analysis of the various techniques used to predict MDD is discussed. Section III elaborates on the entire overview of the designed methodology for the model. The experimental setup is presented in Section IV, followed by a detailed discussion of the results obtained with concluding remarks and future scope in Section V.

II. LITERARY SURVEY

The subject's age and medical history, which are typically absent and have an impact on the diagnosis process and delay the person's early treatment, are key factors that determine how the subject will behave. As a result, objective neuroimaging biomarkers (also known as "neuro markers") have the benefit of being clinically unbiased, which inspires researchers to use a subject's EEG as a tool to screen for various mental disorders like Alzheimer's disease [22], depression, anxiety, and seizures.

The majority of the research focused on using EEG signals to analyze depression, and it typically included feature extraction or raw, preprocessed EEG signals for training models. In [6], nearly 33 participants' resting-state EEG records are used to develop a DeprNet, a CNN model (18 Normal and 15 MDD). This convolution model achieved a maximum accuracy of 91% for subject-wise split data and 99% for record-wise split data.

Similarly in [8], a CNN-LSTM is used to analyze single-channel EEG data from the right and left hemispheres of the brain in experiments with a sample size of 30 participants. Despite the accuracy being 97.66%, the author claimed that the main issue was computational complexity. For the same dataset, a CNN model with 13 convolutional layers and a 95.49% accuracy is obtained [23]. In [24], a model with 6 CNN layers structure is touted as being more effective and less complex. An exhaustive survey on different current DNN models built on EEG-based MDD prediction is presented in [25].

The researchers either work on the raw EEG signals or on the extracted features from the signal. These studies focus on searching for different linear or non-linear patterns to identify MDD. An exhaustive analysis of all previous research, particularly models built on quantitative biomarkers from EEG and characteristics analyzed and tabulated in TABLE.1.

III. METHODOLOGY

Continuously fluctuating EEG data differs from subject to subject and channel to channel, demanding the use of an unsupervised technique to minimize the impact of EEG variation

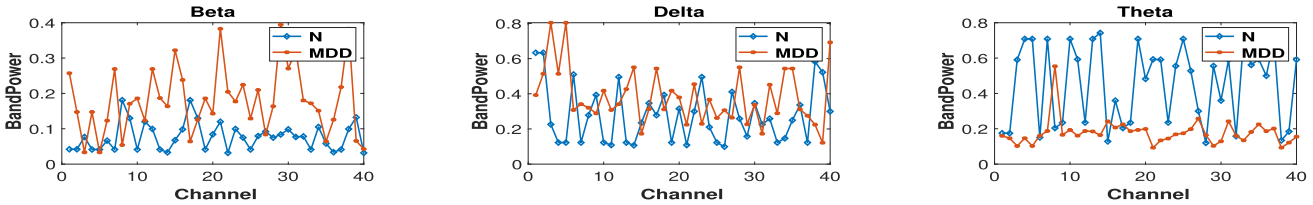

FIGURE 2. Trends between several biomarkers that were recovered from MDD and normal subjects using (a) Beta (b) Delta (c) Theta.

on the detection outcomes. The proposed unsupervised framework is developed employing the linear and non-linear EEG biomarkers to effectively and efficiently address the issues and help in primary diagnosis.

A. NOISE REMOVAL

Noise and artifacts are always present in the raw EEG data that are obtained as a result of a subject's brain activity. Raw data is processed through a band-pass filter adjusted at a frequency of 0.5–40Hz to remove high-frequency noise and rapid spikes, and a 50Hz notch aids in the removal of residual low-frequency noise signals. Independent Component Analysis (ICA) [26] eliminates artifacts produced in the signal due to any slight body movement or changes in the recording device's voltage.

B. BIOMARKERS EXTRACTION

Biomarkers are frequently used to refer to signal qualities or properties that are statistically quantified as indicators for particular biological or pathological processes. The authors have extracted a total of six biomarkers to account for the linear and non-linear features of EEG data. TABLE 2 contains a comprehensive parametric analysis of each of the six biomarkers.

- **BANDPOWER**
  EEG signals are separated into five distinct spectral frequencies, including Alpha, Beta, Gamma, Theta, and Delta. We can parameterize the impact of a certain frequency band on a biological activity under investigation by measuring the relative bandpower of these frequency bands. Welch's Periodogram [27] is used to calculate the bandpower of in-deterministic and fluctuating EEG signals. In the method applied, non-stationary EEG signals are windowed (ω_n) into brief data segments of size K with the assumption that the EEG data will remain stationary within that particular time frame. Then, using Equation(1), the power spectral density (S_x) of these brief periods is computed.

$$S_x(\omega_n) \triangleq \frac{1}{K}\sum_{j=0}^{K-1} P_{x_j,J}(\omega_n) \tag{1}$$

  The periodogram for the Jth time period is denoted here by P. Welch's periodogram is considered computationally efficient for analyzing bandpower as it employs Fast Fourier Transform (FFT).

$$RP = \frac{\int_{-\infty}^{\infty}[S_x(\omega_n)]_{frequency\ band}}{\int_{-\infty}^{\infty}[S_x(\omega_n)]} \tag{2}$$

  The relative band strengths (RP) of three different frequency ranges (Beta, Delta, and Theta) are used to conduct this analysis. Alpha and Gamma are not included here as we could not find an evident change in the values for MDD and N subjects. According to the findings from Fig. 2, the Beta, Delta, and Theta bands were more effective discriminators for MDD subjects than the Alpha band. In subjects with MDD, there is an increase in the power of the Theta band and the Beta band, while the right hemisphere also showed the same trend. There appears to be a correlation between the Theta and Beta bands in people with MDD [12].
- **SIGNAL EXTRACTED FEATURES**
  - **Detrended Fluctuation Analysis:**
    Signals or objects are said to be self-similar if there are components that are identical to the item exactly or roughly, or if the component is statistically similar across scales. A non-stationary, fluctuating signal's long-range correlation parameter can be calculated using DFA [28], a scaling analysis. The entire DFA analysis of an EEG signal is described in the Algorithm 1. This analysis dynamically adjusts the window size along a logarithmic scale as the input size varies. Additionally, a first-degree polynomial is used to fit the detrended data.

Algorithm 1 DFA

1: **Input**: Raw EEG Signal: $x = \{x_1, x_2, \ldots, x_N\}$
2: Detrended signal $y(r) = \sum_i^r (x_i - \bar{x})$.
3: Non-overlapping Segments $2K_s$:Length s.
4: Variance $F_s^2(K)$ for each segments.
5: **Output**: Deterended Fluctuation $F(s)$

$$F(s) = \sqrt{\frac{1}{2K_s}\sum_{n=1}^{2K_s} F_s^2(K)} \tag{3}$$

- **Higuchi's Fractal Dimension:**
  The statistical complexity metric known as a fractal dimension (FD) investigates the impact of sample size on the dynamics of a complicated time series's features through space and time. The Algorithm 2 offers instructions on how to apply Higuchi's algorithm [29] to EEG signals. Through observations, it is found that the divergences in the HFD values are least observed in the subject's Channel-Wise data.

Algorithm 2 HFD

1: **Input**: Raw EEG Signal: $\varkappa = \{\varkappa_1, \varkappa_2, \ldots, \varkappa_N\}$
2: New sub time series are computed y_b^a, such that $a \in \{1, \ldots, K_{max}\}$.
3: Where $y_b^a = \{y(a), y(a+b), y(a+2b), \ldots, y(a+\frac{N-a}{b}.b)$
4: Compute length $l_b(a)$ of each new time series, y_b^a.
5: Compute length of the curve, $l(b) = \frac{N-1}{[\frac{N-a}{b}]b^2} \sum_{i=1}^{[\frac{N-a}{b}]} |x(a+ib) - x(a+(i-1)b)|$
6: Slope H for the straight line $(ln(1/b), ln\,(l(b)))$.
7: **Output**: H

- **LZC:**
  The Lempel-Ziv algorithm [30], which is described in Algorithm. 3, comprehends the complexity or unpredictability of an EEG signal, which is the consequence of scalp activity. It is assessed by the analysis of binary sequences of the signal. For each subject, the provided EEG data $\varkappa$ is altered in a binary sequence $(B) : \{b_1, b_2, b_3, \ldots, b_n\}$.

Algorithm 3 LZC

1: **Input**: EEG signal into Binary Sequence B
2: Divide the B into two sub-word SQ; SQ_π last term omitted.
3: Fixed Prefix $Q \notin v(SQ_\pi)$.
4: Increment complexity counter $c(n)$ normalize C_{LZC} it as [30], [31]
5: **Output**: C_{LZC}

Along with HFD and LZC, DFA has been recognized as a potential discriminator. According to Fig. 3a, depression is associated with lower DFA values as well as a noticeable dip for MDD subjects. The study conducted in [32] also reported similar conclusions. In HFD, an opposite trend is examined. According to Fig.3b, a higher value is observed in subjects with MDD. Although Fig.3c shows a rise in values. A similar conclusion was drawn in [33].

C. GRAPH THEORY AND SPECTRAL CLUSTERING APPROACH

The graph approach is widely accepted in understanding the hidden data characteristics and the various abnormalities. Through, graph brain mapping is more easily done. To effectively understand the brain network, the EEG captured is represented as a graph(G), which is a rudimentary representation of the brain topology. Here, the (V) vertices (or nodes) are connected to the (E) edges (or links). Thus, $G = (V, E)$. To study, the human brain nodes represent brain regions (i.e. EEG electrodes/sensors) while edges are links of associations (i.e. features or connections). The various steps are shown in Fig.4.

- **Defining the vertices in brain network** The brain network's vertices (or nodes) significantly play an important role in the outcome and the analysis of the brain functionality [34]. The nodes are defined in the network using two approaches and we have implemented both of them in our study. The first is "individual channel" which relies on the predefined standard placements of the EEG electrodes on the scalp [35]. This is implemented using the Channel-wise data matrix. The second approach is based on EEG source connectivity that can be implemented by subdividing the scalp into various regions-of-interest [36]. This is done using the Hemisphere-wise matrix.
- **Defining the Edges** The edges are connections between the various electrodes or brain regions. It showcases the various patterns of connectivity and relationship among brain activity. In our study, the edges are defined using correlation among the individual channels and the two hemispheres through a tuple of the five different features extracted above.
- **Compute the connectivity matrix** (W) The connectivity matrix is also commonly known as the adjacency matrix. It defines the information regarding the associations among connectivity patterns. The size of the matrix in our study is CC in which the rows (i) and columns (j) denote nodes, and matrix entries (e_{ij}) denote edges.

$$W = \begin{cases} e_{ij} & \text{if } (v_i, v_j) \in E \\ 0 & \text{if } i == j \\ \text{inf} & \text{otherwise} \end{cases} \tag{4}$$

The connectivity matrix is as shown below:

$$W = \begin{Vmatrix} e_{11} & .. & .. & e_{1C} \\ .. & e_{22} & .. & .. \\ .. & .. & .. & .. \\ e_{C1} & .. & .. & e_{CC} \end{Vmatrix} \tag{5}$$

In our analysis, the binarization of the connectivity matrix is not done using any manual threshold condition. This matrix with the weights on the edges is directly fed to the next step of clustering using the spectral method.

- **Analysis of the Graph using Spectral Clustering** The graph constructed for three data matrix are shown in Fig.12. Through this graph, an interconnection among the various channels is showcased in different cases. Here, each node is a channel, and the connection or (link) is generated based on the W. In the case of Fig.12. (b) and Fig.12. (c) are for the Left and Right hemispheres.

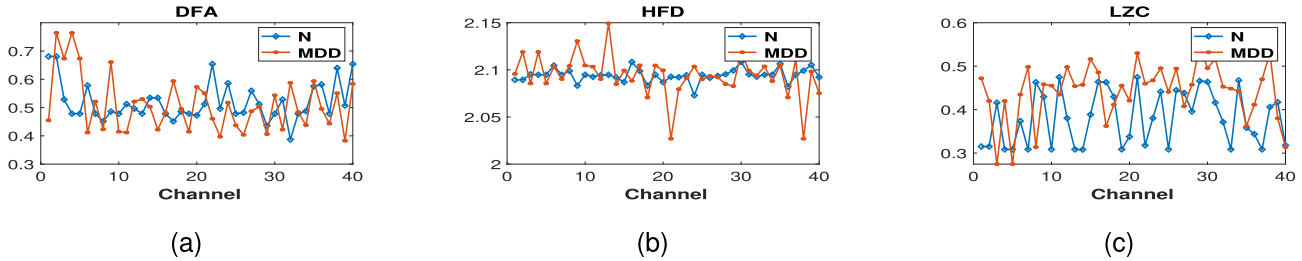

FIGURE 3. Trends between several signal features that were recovered from MDD and normal subjects using (a) DFA, (b) HFD, and (c) LZC.

Here, we observe two separate graphs each for MDD and N subjects. This showcases the bifurcation of channels between the two classes. After the similarity matrix is created. Then normalized spectral clustering specified in the Algorithm 4 is carried out. One of the important steps in spectral clustering is Eigen decomposition, sometimes called spectral decomposition, which is the factorization of the L_{norm} into eigenvalues and vectors [37]. In the case of object clusters, this decomposition is used as the function of cost minimization. Spectral clustering offers an attractive alternative approach, where cluster data use eigenvectors of a similarity matrix derived from the original dataset.

Algorithm 4 Spectral Clustering

1: **Input**:Channels:C, EEG (Data Matrices): D,
2: Similarity Matrix W_{ij}
3: Laplacian matrix: L

$$L = \lambda - W \tag{6}$$

Here λ is the diagonal matrix with the elements

$$\lambda = \sum_{k=1}^{j} W_{ij} \tag{7}$$

The normalized Laplacian matrix is

$$L_{norm} = \lambda^{-\frac{1}{2}} L \lambda^{-\frac{1}{2}} \tag{8}$$

4: Eigenvectors $u_1, \ldots\ldots u_z$
5: Let $U \in R^{C \times z}$ eigenvector columns
6: K-means algorithm on U with mean μ_j

$$K_j = arg_i min \sum_{j=1}^{k} \sum_{W \epsilon U} ||W - \mu_j||^2 \tag{9}$$

7: **Output**: Clusters Z_1 and Z_2

IV. EXPERIMENTAL RESULTS AND DISCUSSION

A. ENVIRONMENTAL SETTINGS

The simulation platform employed is Python 3.6.9 (Google Colab platform) and Matlab R2021a. Packages MNE-Python [26], eeglib [38], and Yet Another Spindle Algorithm (YASA) [39] are used to preprocess the raw EEG signals and extract the necessary features. Table.3 lists the system requirements. In order to make it easier for other researchers to replicate the results, the code will be made publicly available on GitHub after publication.

B. EEG DATA

The data employed for study in this is compiled by Mumtaz [40] University of Sains Malaysia Hospital (HUSM). 62 people with major depressive disorder and 58 normal subjects have been monitored and recorded their EEG for at least a 5-minute. In order to record these, 10-20 electrodes in a standard locations system are used. The data is recorded across twenty channels (FP1, FP2, F7, F3, FZ, F4, F8, T3, C3, CZ, C4, T5, P3, PZ, P4, T6, A2-A1, O1, and O2) under two conditions, only the Eyes Closed (EC) and Eyes Open (EO).

C. DATA MATRICES FORMATION

The Data Matrix designed to be fed in the model design has the size of 120 × 6 (with 120 subjects and six features). There are three distinct Data matrices for analysis: Mean, Channel-wise, and Hemisphere-wise. As a result of averaging, a mean Data Matrix is constructed for all the features derived from each subject using the raw EEG data overall 20 channels. Channel-wise data is made for each channel, containing the respective channel's feature data of all the 120 subjects. Hemisphere-wise data is further considered to compare and contrast taking place in each hemisphere (Left and Right of the brain). Data Matrix for the left hemisphere incorporates averaging the feature data from the EEG channels {FP1 - T5} for each subject. At the same time, the Data Matrix corresponding to the right hemisphere is taken into account by averaging EEG channels' feature data {FP2 - T6}. The mathematical description is presented in Table.4.

D. PARAMETERS FOR ANALYSIS

The results are analyzed in terms of classification as well as clustering. Thus, the evaluation parameters for both are considered. The first classification metric is discussed followed by clustering.

- **Confusion Matrix**
  A confusion matrix, also known as an error matrix, is used to evaluate the performance of a supervised

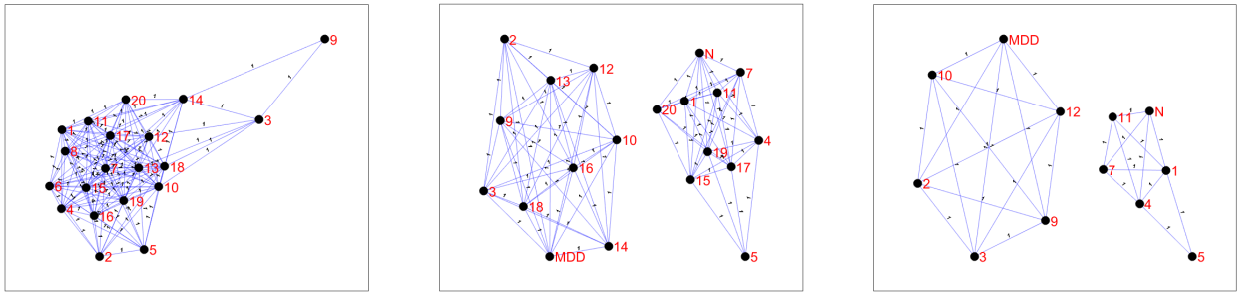

FIGURE 4. Spectral clustering of an EEG signal.

TABLE 2. Overview of the designed framework parametrically.

Processing Block	Input Variables	Settings	Algo/Eq.No	Support Package
Pre-Processing Modules (Filtering and Normalization)	Filter	Band Pass		MNE - python
	Artifact Removal	ICA		
	LPF	0.1 Hz		
	HPF	70 Hz		
	Filter length	Sample Size 1691 (6.605sec)		
Bandpower (BP)	Freq. of Sampling	256Hz	((1)), (2)	YASA
	Window size	4 seconds		
	Method for averaging periodogram	Welch's		
	Bands	Delta = 1-4 Hz, Theta = 4-8 Hz, Beta =12-30 Hz		
Detrended Fluctuation Analysis (DFA)	Min. window size	4 seconds	Alg. 1	eeglib
	WS_{min}	$\frac{Filter\ length}{4}$		
	WS_{max}	$log_2(Filterlength)$		
	Fit-degree	1		
Higuchi's Fractal Dimension (HFD)	k_{max}	$\frac{WS}{4}$	Alg. 2	eeglib
Lemple -Ziv Complexity (LZC)	Signal Threshold	M' (MEDIAN) EEG Samples	Alg. 3	eeglib
Spectral Clustering	No. of Cluster	2	Alg. 4	2021a MATLAB Version
	No. of iteration	1000		
K-means	No. of Cluster	2	(9)	2021a MATLAB Version
	No. of iteration	1000		

TABLE 3. System specifications.

Name	Parameter
System RAM	8GB
CPU	Intel(R) i7 Quad Core, CPU Speed 2.70 GHz
Graphic Processor	HD Graphics card of Intel(R)
Platform	Colab Notebook and MATLAB Version 2021a
Language	Python Version 3.6.9

model by comparing the predicted output of the model to the actual output. The matrix has four different categories, namely true positives a, false positives c, true negatives b, and false negatives d. Here, a represents the number of true positives (correctly predicted positive instances), c represents the number of false positives (incorrectly predicted positive instances), b represents the number of true negatives (correctly predicted negative instances), and d represents the number of false negatives (incorrectly predicted negative instances).

The confusion matrix is an important tool for evaluating the performance of any model. The following are the advantages of it a) **Detailed breakdown of predictions**: The confusion matrix provides a detailed breakdown of the predictions made by the model, including the number of true positives, false positives, true negatives, and false negatives. This information can be used to understand the strengths and weaknesses of the model and to identify areas for improvement. b) **Helps in identifying the impact of misclassifications**: By analyzing the different types of misclassifications (false

TABLE 4. Mathematical description of data matrices.

Nomenlecture	Size (120×6)	Description
Mean	$D=\begin{Bmatrix} S_{11} & S_{12} & .. & .. & S_{16} \\ .. & & & & .. \\ .. & & & & .. \\ .. & & & & .. \\ S_{120.1} & .. & .. & .. & S_{120,6} \end{Bmatrix}$	$[D_1]=\frac{1}{C}\sum\{\ S_{1F}\quad S_{1H}\quad S_{1LZC}\quad S_{1BP_\alpha}\quad S_{1BP_\beta}\quad S_{1BP_\xi}\ \}$
Channel-wise	$D_{FP1}=\begin{Bmatrix} S_{11} & S_{12} & .. & .. & S_{16} \\ .. & & & & .. \\ .. & & & & .. \\ .. & & & & .. \\ S_{120.1} & .. & .. & .. & S_{120,6} \end{Bmatrix}$	$S_1=\{\ S_{1F}\quad S_{1H}\quad S_{1,LZC}\quad S_{1BP_\alpha}\quad S_{1BP_\beta}\quad S_{1BP_\xi}\ \}$
Hemisphere-wise	$D_{LEFT/RIGHT}=\begin{Bmatrix} S_{11} & S_{12} & .. & .. & S_{16} \\ .. & & & & .. \\ .. & & & & .. \\ .. & & & & .. \\ S_{120.1} & .. & .. & .. & S_{120,6} \end{Bmatrix}$	$D_{LEFT}=\begin{Bmatrix} S_{1,FP_1} \\ S_{2,FP_1} \\ .. \\ .. \\ S_{120,}FP_1 \end{Bmatrix}=\{FP_1\text{-}T_5\}$

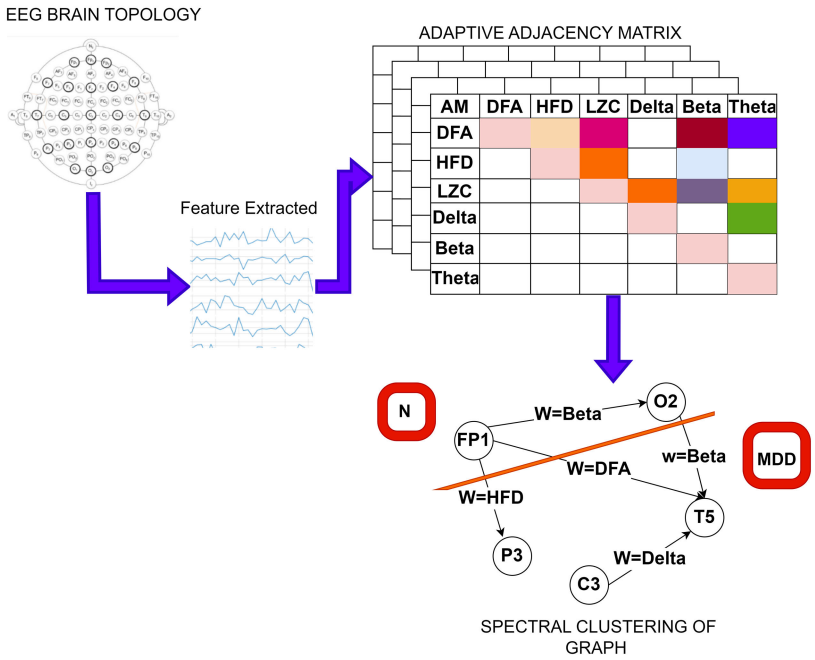

FIGURE 5. Whisker plot for (a) Mean data matrix, (b) Left and (c) Right regions of the brain.

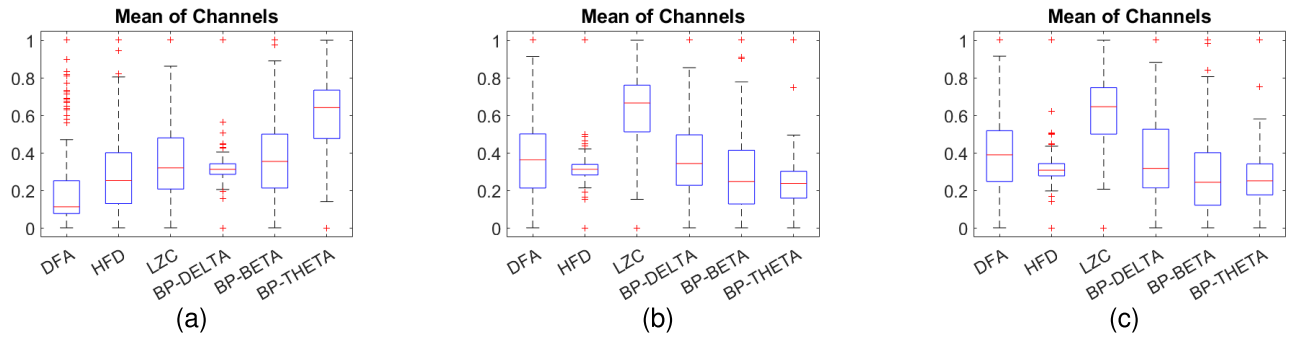

FIGURE 6. Extracted features for left hemisphere with normal subjects.

positives and false negatives), we can determine the impact of each type of error on the overall performance of the model. c) **Enables the selection of appropriate performance metrics**: The confusion matrix provides the necessary information to calculate a range of performance metrics, such as accuracy, precision,

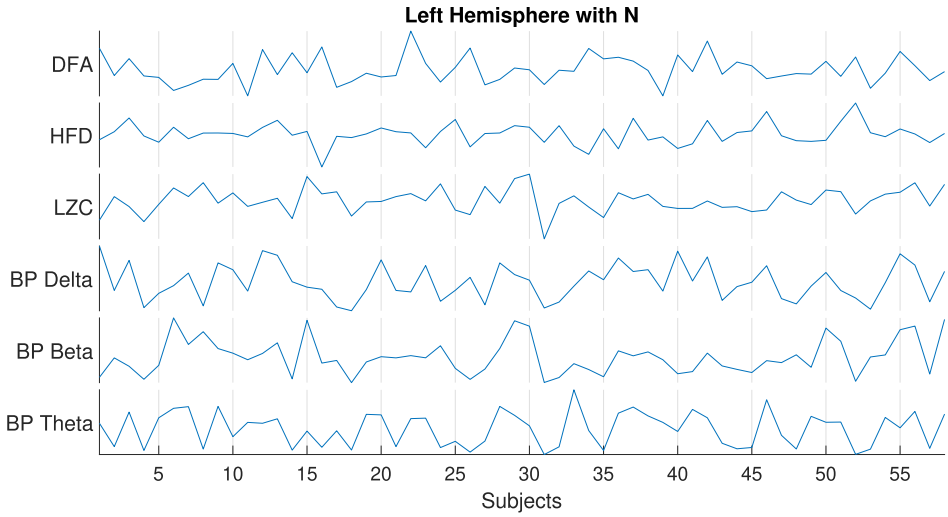

FIGURE 7. Extracted features for left hemisphere with MDD subjects.

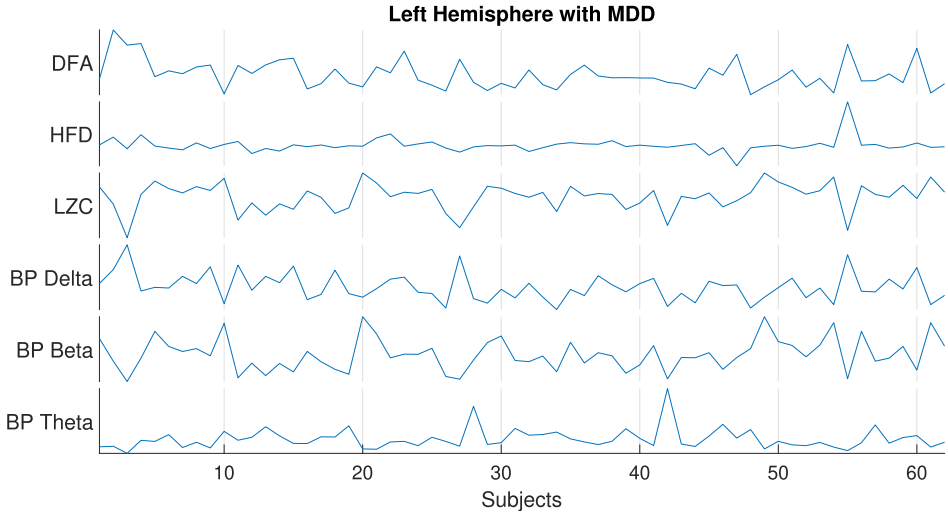

FIGURE 8. Correlation analysis (a) FP1 Channel and (b) Mean data matrix. (The values in red indicate which pairs of variables have correlations significantly different from zero).

TABLE 5. A comparative study of the classification parameters with the existing state of art methods.

Model	Biomarkers	LH			RH		
		Acc (%)	Sen(%)	Spec(%)	Acc (%)	Sen (%)	Spec (%)
CNN-LTSM model [8]		97.66%	97.03%	98.27%	99.12%	98.55%	99.79%
Enhanced - PNN [45]		98.20%	97.10%	99.40%	99.50%	99.20%	99.70%
13-layer CNN [23]		93.54%	91.89%	95.18%	95.96%	94.99%	96.00%
PROPOSED MODEL							
Spectral Clustering Method	4	**98%**	95%	100%	**99%**	97%	97%
	6	87%	87%	86%	93%	94%	93%
K-Means	4	61%	82%	38%	38%	19%	59%
	6	24%	23%	26%	25%	26%	24%

*The bold faces values show the best achieved.

recall, and F1 score. These metrics can be used to evaluate the performance of the model and to compare different models. d) **Helps in fine-tuning the model**: The information provided by the confusion matrix can be used to fine-tune the model, such as adjusting the decision threshold, changing the feature

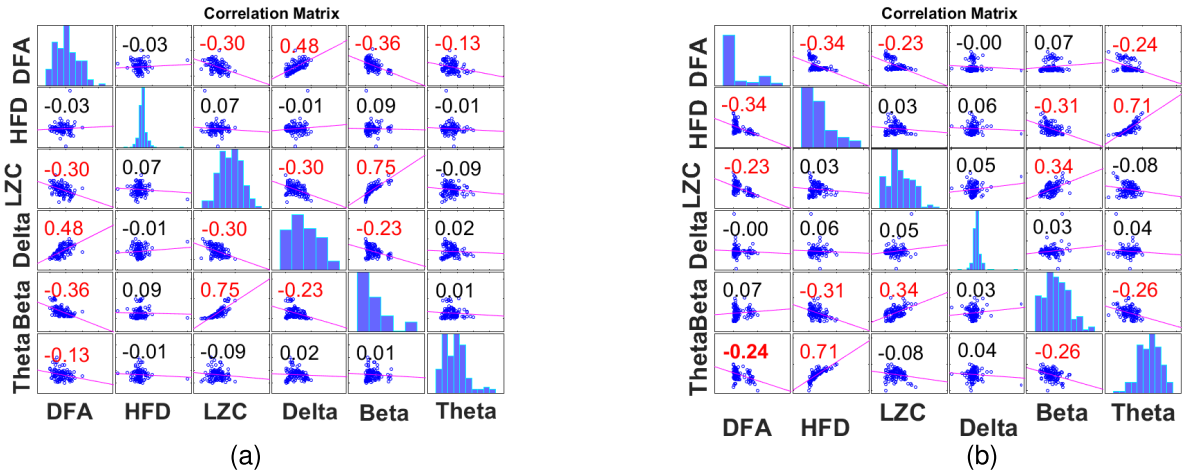

FIGURE 9. Unsupervised classification of the labels for left hemisphere data matrix.

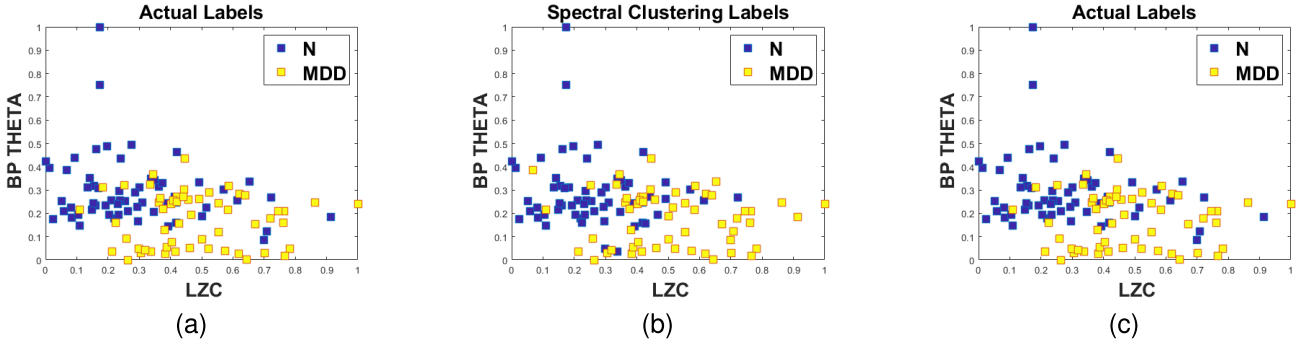

FIGURE 10. Unsupervised classification of the labels for right hemisphere data matrix.

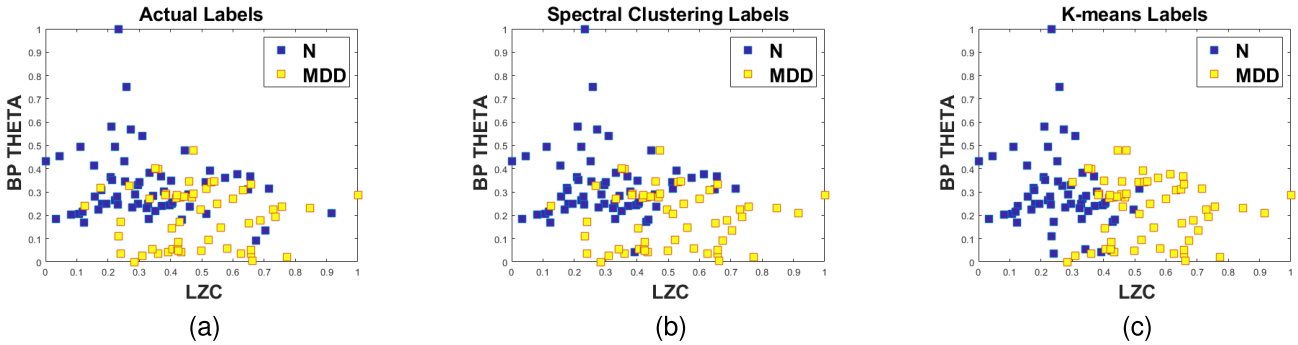

FIGURE 11. Unsupervised classification of the labels for mean data matrix.

selection, or using a different algorithm altogether. This can help to improve the overall performance of the model.

- **Accuracy** Accuracy, in terms of correct label match, refers to the proportion of instances in a dataset for which the model's prediction matches the actual (correct) label.

$$Acc = \frac{a+b}{a+b+c+d} \tag{10}$$

- **Sensitivity**

Sensitivity, also known as recall or true positive rate, is a performance metric derived from a confusion matrix that measures the proportion of positive instances that are correctly identified by the model. In other words, sensitivity measures the model's ability to correctly identify positive instances. Mathematically, sensitivity can be defined as follows:

$$Sen = \frac{a}{a+d} \tag{11}$$

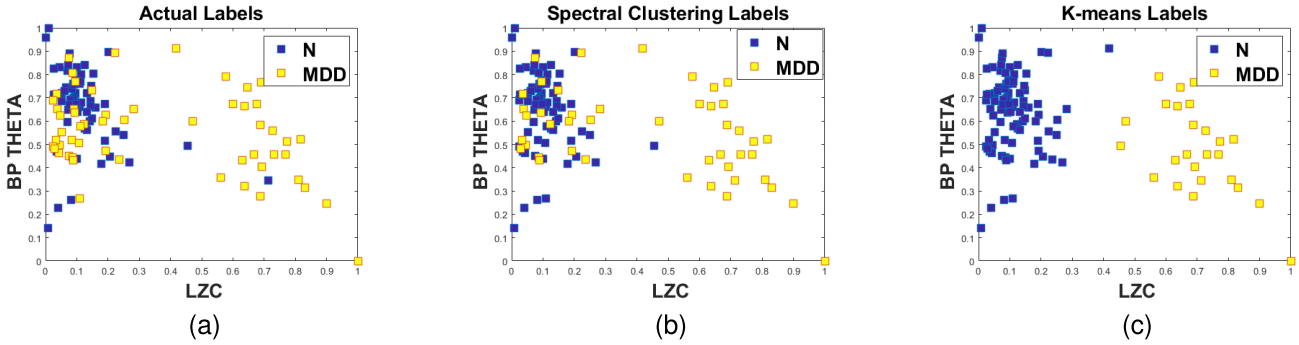

FIGURE 12. Graph brain network for a) Mean data matrix, b) Left hemisphere, and c) Right hemisphere.

TABLE 6. Time complexity study of the proposed method with other state of art in literature.

Method	Time to Train (sec)	Time to Test (msec)	Subjects
S-SVM [46]	21888	0.015	1
CNN-LTSM [8]	52	5.000	1
CNN-DeprNet [6]	2256	3.600	1
H-KNN [9]	36956	0.013	1
H-DBN [47]	29604	0.096	1
S-EMD [48]	18920	0.056	1
PROPOSED CLUSTERING MODEL (1000 Iterations)			
Spectral	**0**	**120.005**	120
K-means	**0**	**100.392**	120

*The bold faces values show the best achieved.

Sensitivity is an important metric, especially in problems where correctly identifying positive instances is critical, such as in medical diagnosis. A high sensitivity means that the model is able to correctly identify most of the positive instances in the dataset, while a low sensitivity indicates that the model is missing many of the positive instances.

- **Specificity** Specificity is a performance metric derived from a confusion matrix that measures the proportion of negative instances that are correctly identified by the model. In other words, specificity measures the model's ability to correctly identify negative instances. Mathematically, specificity can be defined as follows:

$$Spec = \frac{b}{b+d} \tag{12}$$

Specificity is an important metric, especially in problems where correctly identifying negative instances is critical. A high specificity means that the model is able to correctly identify most of the negative instances in the dataset, while a low specificity indicates that the model is incorrectly identifying many of the negative instances as positive.

The quality of input datasets plays a crucial role in the assessment of clustering algorithms. Clustering validity indices use two features to help interpret the clusters produced in a cohort: compactness and separability. D is the Data Matrix for any of the three cases designed as in the Subsection. C and shown in Table.5. These are clustered in two clusters Z_1 and Z_2. The following different metrics are used to evaluate these groups.

- **RI**
  In this index, instead of investigating the correlation between the correct labels and those that get assigned, it evaluates the relationship between points within the datasets [41]. It is also suitable for unsupervised approaches because it can be utilized without labels. Mathematically, an index is defined in Eq.(13) as the ratio of the frequency of agreements to the total number of pairs matched. The index lies in the range $ri \in [0, 1]$, where, 0 is the index of disagreement and 1 for similarity. nC_2 is the total number of terms classified.

$$ri = \frac{a+b}{nC_2} \tag{13}$$

- **ARI**
  With ARI, you can easily and effectively get the results compared with K-means (the blob shape being isotropic) to those achieved by spectral clustering algorithms (normally in ''folded'' shapes) without making any assumptions about the cluster structure. ARI [42] is formulated as shown in Eq.(14).

$$ARI = \frac{ri - Ex(ri)}{max(ri) - Ex(ri)} \tag{14}$$

- **Classification Error Percentage (CEP)**
  The number of labels that the desired model misidentified for the chosen clustering approach is shown by (CEP). The clustering method labels and the original labels are contrasted. Mathematically, CEP is Eq.(15) [43]

$$CEP = \frac{MissClassifiedPattern}{TotalPatterns} \tag{15}$$

E. EXPERIMENTAL STUDY AND DISCUSSION

Experimental validation is done to investigate the various aspects of the study. The various data matrix as showcased

TABLE 7. Designed framework accuracy analysis for channel-wise data.

Channel	Spectral Clustering					K-means				Guohun Zhu et. al. [45]		
Parameters	Acc (%)	Sen (%)	Spec (%)	ARI	RI	CEP	Acc (%)	Sen (%)	Spec (%)	ARI	RI	CEP	Acc (%)	Sen (%)	Spec (%)
Mean	90	98	81	0.6371	0.8185	0.1000	30	59	59	0.1549	0.5765	0.7000	-	-	-
FP1	**96**	**92**	**100**	**0.8389**	**0.9195**	**0.0417**	61	50	72	0.0392	0.5195	0.3917	86.8	0.88	0.85
F3	88	77	100	0.5844	0.7922	0.1167	62	61	62	0.0464	0.5232	0.3833	85.2	0.82	0.88
C3	95	94	97	0.8084	0.9042	0.0500	19	23	16	0.3750	0.6875	0.8083	88.1	0.88	0.88
P3	93	92	95	0.7490	0.8745	0.0667	20	23	17	0.3545	0.6773	0.8000	86.6	0.84	0.89
O1	85	95	74	0.4859	0.7429	0.1500	21	18	24	0.3347	0.6674	0.7917	88.4	0.90	0.87
F7	87	74	100	0.5341	0.7669	0.1333	34	35	33	0.0926	0.5464	0.6583	88.4	0.90	0.87
T3	86	87	84	0.5095	0.7548	0.1417	30	26	34	0.1529	0.5765	0.7000	88.0	0.94	0.82
T5	93	97	88	0.7202	0.8601	0.075	21	19	22	0.3347	0.6674	0.7917	88.3	0.87	0.89
FZ	64	85	41	0.0739	0.5363	0.3583	69	58	81	0.1400	0.5699	0.3083	84.0	0.84	0.84
FP2	57	68	45	0.0099	0.5048	0.4333	42	47	36	0.0196	0.5098	0.5833	88.5	0.89	0.88
F4	52	73	29	-0.0060	0.4964	0.4833	33	44	21	0.1153	0.5576	0.6750	85.3	0.90	0.81
C4	93	95	91	0.7490	0.8745	0.0667	25	31	17	0.2608	0.6304	0.7583	84.7	0.89	0.81
P4	90	90	90	0.6370	0.8185	0.1000	18	24	12	0.3960	0.6980	0.8167	88.4	0.88	0.89
O2	89	92	86	0.6104	0.8052	0.1083	25	26	24	0.2436	0.6218	0.7500	84.8	0.89	0.81
F8	**96**	**92**	**100**	**0.8389**	**0.9195**	**0.0417**	43	48	36	0.0143	0.5071	0.5750	85.9	0.89	0.82
T4	61	52	71	0.0391	0.5195	0.3917	33	32	34	0.1035	0.5518	0.6667	89.2	0.87	0.91
T6	94	90	98	0.7784	0.8892	0.0583	24	18	31	0.2608	0.6304	0.7583	86.9	0.86	0.88
CZ	84	74	95	0.4626	0.7312	0.1583	36	37	34	0.0724	0.5363	0.6417	86.9	0.83	0.91
PZ	93	90	97	0.7490	0.8745	0.0667	17	24	9	0.4398	0.7199	0.8333	87.2	0.86	0.88
A2-A1	68	94	40	0.1170	0.5576	0.3250	62	79	43	0.0473	0.5232	0.3833	-	-	-

*The bold faces values show the best achieved.

in Table.4 is provided to the model. The designed model is based on spectral clustering, the hyper-parameters for this algorithm is the number of clusters. Also, to compare our results with other standard and fast clustering algorithms K-means is taken. The hyper-parameters tunned in K-means are the number of iterations, the number of clusters, and the method of cluster initialization. The number of iterations is taken as 1000, and the number of clusters is chosen using the Elbow method. The method for initialization is to take a random selection of seeds for centroids.

In Fig.5, an underlying statistical distribution of various biomarkers is demonstrated graphically. The observations are: (a) The Mean Data Matrix has a higher proportion of outliers than hemisphere-wise data. Compared to the left and right hemispheres' respective accuracy rates of 95% and 77%, the Mean Data Matrix's overall accuracy for spectral grouping is 90%. (b) For the right hemisphere compared to the left, the data is more skewed. Through the box plot, it is observed that the distribution is heavy-tailed and this eventually affects the node partitioning in spectral clustering. This is also evident in the results tabulated in Table. 8. In spectral clustering results values for *ARI* and *RI* are reported higher for the left in contrast to the compared to the right. The overall Data Matrix is not normally distributed, being skewed as a result of which K-means accuracy drastically decreases although being less computationally complex and simple than spectral clustering.

The distribution of features extracted for the Left hemisphere for the Normal subject is shown in Fig.6 and for MDD in Fig.7. The observation is: DFA has more crest and valley than Normal as compared to MDD subjects. Similarly, HFD is flat for MDD subjects. An evident difference is observed between both the feature set that can be utilized to get the clusters.

The inter-dependency between the hemispheres and individual channels is examined through a correlation study. The results for two cases: the channel (FP1) and the Mean Data Matrix are shown here. There is a visible change in the correlation between biomarkers. The inferences drawn from Fig.8 are: (a) Beta Band Power is uncorrelated to HFD while linearly related to LZC. (b) DFA and Delta Band Power are positively correlated. (c) while the remaining features demonstrate no relationship among them. In Fig.8 for Mean Data Matrix prominent conclusions are: (a) Beta Band Power is uncorrelated to all the other features while having a small positive relation with LZC. (b) Theta Band Power and DFA are having a linearly increasing and decreasing relationship with HFD respectively.

The methodology is also compared with the other existing methods in the literature in terms of Hemisphere-wise accuracy and time complexity. The works compared have also tested their models on the same dataset. The accuracy is compared in Table.5. The method proposed has achieved 98% accuracy in the left hemisphere and 97% in the right hemisphere. A comparison of the time complexity of different

TABLE 8. Cluster analysis for biomarkers on hemisphere-wise data.

Hemisphere	Biomarkers	Spectral Clustering			K-means		
Parameters		ARI	RI	CEP	ARI	RI	CEP
Left	4	0.9017	0.9508	0.0250	0.5195	0.3917	0.0403
	6	**0.8339**	**0.7669**	**0.1333**	**0.6304**	**0.7583**	**0.2608**
Right	4	0.8700	0.9350	0.0333	0.5232	0.6167	0.0476
	6	**0.7490**	**0.8745**	**0.0667**	**0.6218**	**0.7500**	**0.2437**

*The bold faces values show the best achieved.

proposed models is tabulated in Table. 6. The proposed method takes no time for testing as its unsupervised. In this model, as the data is given, the graph is constructed for the whole data at once and results get displayed. In case, any new subject is introduced. The subject's features will be mapped on the current centroid information of the existing clusters and a nearby centroid will be assigned to the new subject.

The role of EEG captured through individual channels is also important to understand. In Table.7 various parameters pertaining to the classification and unsupervised clustering are investigated. The general observations drawn are: The maximum accuracy is recorded for channel FP1; with $ARI = 0.8389$ and $CEP = 0.0417$. This channel is normally associated with cogitative, memory and perceptions of an individual. The other extreme reported is for channel F4 with negative values of $ARI = -0.0060$ and $CEP = 0.480$. The clustering of the Mean Data Matrix is shown in Fig.11. The labels are overlapping in nature and not linearly separable for the features LZC and Theta Band Power. Although the results obtained from the K-means algorithm make a clear demarcation and make them linearly separable.The results of the left hemisphere have minimum overlapping as shown in Fig.9 and for the right hemisphere in Fig.10.

Classification accuracy of spectral clustering is more as compared to the K-means. Thus, spectral clustering offers a better solution as compared to K-means. The comparison in terms of the hemisphere is given in Table.8. In both the cases of the hemisphere, the values of *ARI* and *RI* are high which indicates the structure similarity although the *CEP* value maps the original labels with the obtained label. The author also has compared results with the other work carried out on the same dataset using a graph method [44]. It is designed using the oblique visibility graph, then the parameters are given to the standard SVM with RBF kernel for the classification.

V. CONCLUSION

In this article, the model has been designed for the computerized detection of depression that effectively reduces the cost incurred in the annotation of EEG signals. Additionally, there is a reduction in the complexity of time and space involved in training large networks. The primary analysis of any new ailment or brain condition can be easily done with small sample size and in the absence of data labels. This model works on features extracted from the EEG signal along with a few prominent biomarkers. A Data Matrix encapsulates a full mapping of brain activity and its correlation among various areas of the brain. An accuracy of 98% is achieved for the Left hemisphere, whereas the accuracy of the right hemisphere is 97%. Channel FP1 has the greatest improvement in terms of channel accuracy, with a gain of 96%. Additional biomarkers including the Hurst Exponent, Hjorth Complexity, and Spectral Asymmetry Index (SASI) will be investigated in future studies. This method allows a full understanding of the EEG signal. Additionally, it's important to consider how each biomarker influences our general comprehension and accuracy in order to identify a more widely used and uncomplicated spectrum partitioning strategy.

REFERENCES

[1] *Other Common Mental Disorders: Global Health Estimates*, World Health Organization, Geneva, Switzerland, 2017.
[2] S. Grover et al., "Psychological impact of COVID-19 lockdown: An online survey from India," *Indian J. Psychiatry*, vol. 62, no. 4, p. 354, 2020.
[3] L. L. Popa, D. Chira, V. Dăbală, E. Hapca, B. O. Popescu, C. Dina, R. Cherecheş, Ş. Strilciuc, and D. F. Mureşanu, "Quantitative EEG as a biomarker in evaluating post-stroke depression," *Diagnostics*, vol. 13, no. 1, p. 49, Dec. 2022.
[4] D. M. Khan, K. Masroor, M. F. M. Jailani, N. Yahya, M. Z. Yusoff, and S. M. Khan, "Development of wavelet coherence EEG as a biomarker for diagnosis of major depressive disorder," *IEEE Sensors J.*, vol. 22, no. 5, pp. 4315–4325, Mar. 2022.
[5] M. McVoy, S. Chumachenko, F. Briggs, F. Kaffashi, and K. Loparo, "A predictive biomarker model using quantitative electroencephalography in adolescent major depressive disorder," *J. Child Adolescent Psychopharmacol.*, vol. 32, no. 9, pp. 460–466, Nov. 2022.
[6] A. Seal, R. Bajpai, J. Agnihotri, A. Yazidi, E. Herrera-Viedma, and O. Krejcar, "DeprNet: A deep convolution neural network framework for detecting depression using EEG," *IEEE Trans. Instrum. Meas.*, vol. 70, pp. 1–13, 2021.
[7] C.-T. Wu, H.-C. Huang, S. Huang, I.-M. Chen, S.-C. Liao, C.-K. Chen, C. Lin, S.-H. Lee, M.-H. Chen, C.-F. Tsai, C.-H. Weng, L.-W. Ko, T.-P. Jung, and Y.-H. Liu, "Resting-state EEG signal for major depressive disorder detection: A systematic validation on a large and diverse dataset," *Biosensors*, vol. 11, no. 12, p. 499, Dec. 2021.
[8] B. Ay, O. Yildirim, M. Talo, U. B. Baloglu, G. Aydin, S. D. Puthankattil, and U. R. Acharya, "Automated depression detection using deep representation and sequence learning with EEG signals," *J. Med. Syst.*, vol. 43, no. 7, Jul. 2019.
[9] H. Cai, J. Han, Y. Chen, X. Sha, Z. Wang, B. Hu, J. Yang, L. Feng, Z. Ding, Y. Chen, and J. Gutknecht, "A pervasive approach to EEG-based depression detection," *Complexity*, vol. 2018, pp. 1–13, Jan. 2018.

[10] M. Bachmann, L. Päeske, K. Kalev, K. Aarma, A. Lehtmets, P. Ööpik, J. Lass, and H. Hinrikus, "Methods for classifying depression in single channel EEG using linear and nonlinear signal analysis," *Comput. Methods Programs Biomed.*, vol. 155, pp. 11–17, Mar. 2018.

[11] W. Mumtaz, L. Xia, M. A. M. Yasin, S. S. A. Ali, and A. S. Malik, "A wavelet-based technique to predict treatment outcome for major depressive disorder," *PLoS ONE*, vol. 12, no. 2, Feb. 2017, Art. no. e0171409.

[12] W. Mumtaz, L. Xia, S. S. A. Ali, M. A. M. Yasin, M. Hussain, and A. S. Malik, "Electroencephalogram (EEG)-based computer-aided technique to diagnose major depressive disorder (MDD)," *Biomed. Signal Process. Control*, vol. 31, pp. 108–115, Jan. 2017.

[13] U. R. Acharya, V. K. Sudarshan, H. Adeli, J. Santhosh, J. E. W. Koh, S. D. Puthankatti, and A. Adeli, "A novel depression diagnosis index using nonlinear features in EEG signals," *Eur. Neurol.*, vol. 74, nos. 1–2, pp. 79–83, 2015.

[14] B. Hosseinifard, M. H. Moradi, and R. Rostami, "Classifying depression patients and normal subjects using machine learning techniques and nonlinear features from EEG signal," *Comput. Methods Programs Biomed.*, vol. 109, no. 3, pp. 339–345, Mar. 2013.

[15] M. Ahmadlou, H. Adeli, and A. Adeli, "Fractality analysis of frontal brain in major depressive disorder," *Int. J. Psychophysiol.*, vol. 85, no. 2, pp. 206–211, Aug. 2012.

[16] S. Pravin Kumar, N. Sriraam, P. G. Benakop, and B. C. Jinaga, "Entropies based detection of epileptic seizures with artificial neural network classifiers," *Expert Syst. Appl.*, vol. 37, no. 4, pp. 3284–3291, Apr. 2010.

[17] S. M. Alarcão and M. J. Fonseca, "Emotions recognition using EEG signals: A survey," *IEEE Trans. Affect. Comput.*, vol. 10, no. 3, pp. 374–393, Jul. 2019.

[18] H. Adeli, Z. Zhou, and N. Dadmehr, "Analysis of EEG records in an epileptic patient using wavelet transform," *J. Neurosci. Methods*, vol. 123, no. 1, pp. 69–87, Feb. 2003.

[19] S. Olbrich and M. Arns, "EEG biomarkers in major depressive disorder: Discriminative power and prediction of treatment response," *Int. Rev. Psychiatry*, vol. 25, no. 5, pp. 604–618, Oct. 2013.

[20] X. Chen, J. Ji, T. Ji, and P. Li, "Cost-sensitive deep active learning for epileptic seizure detection," in *Proc. ACM Int. Conf. Bioinf., Comput. Biol., Health Informat.*, Aug. 2018, pp. 226–235.

[21] D. Yuan, X. Chang, P. Huang, Q. Liu, and Z. He, "Self-supervised deep correlation tracking," *IEEE Trans. Image Process.*, vol. 30, pp. 976–985, 2021.

[22] D. Kim and K. Kim, "Detection of early stage Alzheimer's disease using EEG relative power with deep neural network," in *Proc. 40th Annu. Int. Conf. IEEE Eng. Med. Biol. Soc. (EMBC)*, Jul. 2018, pp. 352–355.

[23] U. R. Acharya, S. L. Oh, Y. Hagiwara, J. H. Tan, H. Adeli, and D. P. Subha, "Automated EEG-based screening of depression using deep convolutional neural network," *Comput. Methods Programs Biomed.*, vol. 161, pp. 103–113, Jul. 2018.

[24] G. Sharma, A. Parashar, and A. M. Joshi, "DepHNN: A novel hybrid neural network for electroencephalogram (EEG)-based screening of depression," *Biomed. Signal Process. Control*, vol. 66, Apr. 2021, Art. no. 102393.

[25] A. Safayari and H. Bolhasani, "Depression diagnosis by deep learning using EEG signals: A systematic review," *Med. Novel Technol. Devices*, vol. 12, Dec. 2021, Art. no. 100102.

[26] A. Gramfort, "MEG and EEG data analysis with MNE-Python," *Frontiers Neurosci.*, vol. 7, no. 267, pp. 1–13, Jan. 2013.

[27] P. Welch, "The use of fast Fourier transform for the estimation of power spectra: A method based on time averaging over short, modified periodograms," *IEEE Trans. Audio Electroacoustics*, vol. AE-15, no. 2, pp. 70–73, Jun. 1967.

[28] R. M. Bryce and K. B. Sprague, "Revisiting detrended fluctuation analysis," *Sci. Rep.*, vol. 2, no. 1, p. 315, Mar. 2012.

[29] T. Higuchi, "Approach to an irregular time series on the basis of the fractal theory," *Phys. D, Nonlinear Phenomena*, vol. 31, no. 2, pp. 277–283, Jun. 1988.

[30] A. Lempel and J. Ziv, "On the complexity of finite sequences," *IEEE Trans. Inf. Theory*, vol. IT-22, no. 1, pp. 75–81, Jan. 1976.

[31] M. Aboy, R. Hornero, D. Abasolo, and D. Alvarez, "Interpretation of the Lempel–Ziv complexity measure in the context of biomedical signal analysis," *IEEE Trans. Biomed. Eng.*, vol. 53, no. 11, pp. 2282–2288, Nov. 2006.

[32] S. Mahato and S. Paul, "Electroencephalogram (EEG) signal analysis for diagnosis of major depressive disorder (MDD): A review," in *Nanoelectronics, Circuits and Communication Systems* (Lecture Notes in Electrical Engineering), vol. 511. Singapore: Springer, 2019, pp. 323–335.

[33] K. Kalev, M. Bachmann, L. Orgo, J. Lass, and H. Hinrikus, "Lempel–Ziv and multiscale Lempel–Ziv complexity in depression," in *Proc. 37th Annu. Int. Conf. IEEE Eng. Med. Biol. Soc. (EMBC)*, Aug. 2015, pp. 4158–4161.

[34] J. Liu, M. Li, Y. Pan, W. Lan, R. Zheng, F.-X. Wu, and J. Wang, "Complex brain network analysis and its applications to brain disorders: A survey," *Complexity*, vol. 2017, pp. 1–27, Jan. 2017.

[35] R. Oostenveld and P. Praamstra, "The five percent electrode system for high-resolution EEG and ERP measurements," *Clin. Neurophysiol.*, vol. 112, no. 4, pp. 713–719, Apr. 2001.

[36] G. N. Dimitrakopoulos, I. Kakkos, Z. Dai, J. Lim, J. J. de Souza, A. Bezerianos, and Y. Sun, "Task-independent mental workload classification based upon common multiband EEG cortical connectivity," *IEEE Trans. Neural Syst. Rehabil. Eng.*, vol. 25, no. 11, pp. 1940–1949, Nov. 2017.

[37] Z. Khan, P. Fan, S. Fang, and F. Abbas, "An unsupervised cluster-based VANET-oriented evolving graph (CVoEG) model and associated reliable routing scheme," *IEEE Trans. Intell. Transp. Syst.*, vol. 20, no. 10, pp. 3844–3859, Oct. 2019.

[38] L. C. Gómez, "eeglib: A Python module for EEG feature extraction," *SoftwareX*, vol. 15, 2021, Art. no. 100745.

[39] R. Vallat and M. P. Walker, "An open-source, high-performance tool for automated sleep staging," *eLife*, vol. 10, Oct. 2021, Art. no. e70092.

[40] W. Mumtaz, "MDD patients and healthy controls EEG data (new). figshare. [Dataset]," 2016, doi: 10.6084/m9.figshare.4244171.v2.

[41] W. M. Rand, "Objective criteria for the evaluation of clustering methods," *J. Amer. Stat. Assoc.*, vol. 66, no. 336, pp. 846–850, Dec. 1971.

[42] J. E. Chacón and A. I. Rastrojo, "Minimum adjusted Rand index for two clusterings of a given size," *Adv. Data Anal. Classification*, vol. 17, no. 1, pp. 125–133, Mar. 2023.

[43] D. Karaboga and C. Ozturk, "A novel clustering approach: Artificial bee colony (ABC) algorithm," *Appl. Soft Comput.*, vol. 11, no. 1, pp. 652–657, Jan. 2011.

[44] G. Zhu, T. Qiu, Y. Ding, S. Gao, N. Zhao, F. Liu, X. Zhou, and R. Gururajan, "Detecting depression using single-channel EEG and graph methods," *Mathematics*, vol. 10, no. 22, p. 4177, Nov. 2022.

[45] O. Faust, P. C. A. Ang, S. D. Puthankattil, and P. K. Joseph, "Depression diagnosis support system based on EEG signal entropies," *J. Mech. Med. Biol.*, vol. 14, no. 3, Jun. 2014, Art. no. 1450035.

[46] M. Sharma, S. Patel, and U. R. Acharya, "Automated detection of abnormal EEG signals using localized wavelet filter banks," *Pattern Recognit. Lett.*, vol. 133, pp. 188–194, May 2020.

[47] H. Cai, X. Sha, X. Han, S. Wei, and B. Hu, "Pervasive EEG diagnosis of depression using deep belief network with three-electrodes EEG collector," in *Proc. IEEE Int. Conf. Bioinf. Biomed. (BIBM)*, Dec. 2016, pp. 1239–1246.

[48] J. Shen, X. Zhang, G. Wang, Z. Ding, and B. Hu, "An improved empirical mode decomposition of electroencephalogram signals for depression detection," *IEEE Trans. Affect. Comput.*, vol. 13, no. 1, pp. 262–271, Jan. 2022.

SHREEYA GARG received the degree in electronics and communication from Banasthali Vidyapith. Her research interests include artificial intelligence, machine learning, digital signal processing, and related fields.

URVASHI PRAKASH SHUKLA received the bachelor's degree in electronics and communication engineering in 2009, the M.Tech. degree in compressive sensing in 2013, and the Ph.D. degree from NIT, Jaipur, India. Her Ph.D. thesis was on clustering algorithms based on social spider optimization for hyperspectral image analysis. She is currently an Assistant Professor with the Department of Computer Science, Bansanthali Vidhyapith. She has authored or coauthored many articles in reputed journals and conferences. Her research interests include obtaining solution for problems associated with medical signal processing, hyperspectral images, data mining, and artificial intelligence. She is an Active Reviewer of IEEE Access and Elsevier journals.

LINGA REDDY CENKERAMADDI (Senior Member, IEEE) received the master's degree in electrical engineering from IIT Delhi, New Delhi, India, in 2004, and the Ph.D. degree in electrical engineering from the Norwegian University of Science and Technology (NTNU), Trondheim, Norway, in 2011. He was with Texas Instruments, where he was involved in mixed-signal circuit design. After finishing his Ph.D. degree, he was involved in radiation imaging for an atmosphere–space interaction monitor (ASIM mission to the International Space Station) with the University of Bergen, Bergen, Norway, from 2010 to 2012. He is currently the Leader of the Autonomous and Cyber-Physical Systems (ACPS) Research Group, University of Agder, Grimstad, Norway, where he is also a Professor. He is the Principal Investigator and a Co-Principal Investigator of many research grants from the Norwegian Research Council. He has coauthored over 130 research publications that have been published in prestigious international journals and standard conferences. His research interests include the Internet of Things (IoT), cyber-physical systems, autonomous systems, robotics and automation involving advanced sensor systems, computer vision, thermal imaging, LiDAR imaging, radar imaging, wireless sensor networks, smart electronic systems, advanced machine learning techniques, connected autonomous systems, including drones/unmanned aerial vehicles (UAVs), unmanned ground vehicles (UGVs), unmanned underwater systems (UUSs), 5G (and beyond)-enabled autonomous vehicles, and socio-technical systems like urban transportation systems, smart agriculture, and smart cities. He is also quite active in medical imaging. He is also a member of ACM and a member of the editorial boards of various international journals and the technical program committees of several IEEE conferences. Several of his master's students have received the Best Master Thesis Award in information and communication technology (ICT). He serves as a reviewer for several reputed international conferences and IEEE journals.